Time-reversal symmetry breaking in topological superconductor $Sr_{0.1}Bi_2Se_3$

P. Neha,[1] P. K. Biswas,[2,*] Tanmoy Das,[3,*] and S. Patnaik[1,*]
[1]*School of Physical Sciences, Jawaharlal Nehru University, New Delhi-110067, India*
[2]*ISIS Pulsed Neutron and Muon Source, STFC Rutherford Appleton Laboratory, Harwell Campus, Didcot, Oxfordshire-OX110QX, United Kingdom*
[3]*Department of Physics, Indian Institute of Science, Bangalore-560012, India*

(Received 4 October 2018; published 16 July 2019)

The single helical Fermi surface on the surface state of three-dimensional topological insulator Bi_2Se_3 is constrained by the time-reversal invariant bulk topology to possess a spin-singlet superconducting pairing symmetry. In fact, the Cu-doped and pressure-tuned superconducting Bi_2Se_3 show no evidence of the time-reversal symmetry (TRS) breaking. We report on the detection of the TRS breaking in the topological superconductor $Sr_{0.1}Bi_2Se_3$, probed by zero-field μSR measurements. The TRS breaking provides strong evidence for the existence of a spin-triplet pairing state. The existence of TRS breaking is also verified by longitudinal-field μSR measurements, which negates the possibility of magnetic impurities as the source of TRS breaking. The temperature-dependent superfluid density deduced from transverse-field μSR measurements yields nodeless superconductivity with low superconducting carrier density and penetration depth $\lambda = 1622(134)$ nm. From the microscopic theory of unconventional pairing, we find that such a fully gapped spin-triplet pairing channel is promoted by the complex interplay between the structural hexagonal warping and higher order Dresselhaus spin-orbit-coupling terms. Based on Ginzburg-Landau analysis, we delineate the mixing of singlet- to triplet-pairing symmetry as the chemical potential is tuned far above from the Dirac cone. Our observation of such spontaneous TRS breaking chiral superconductivity on a helical surface state, protected by the TRS invariant bulk topology, can open avenues for interesting research and applications.

DOI: 10.1103/PhysRevMaterials.3.074201

I. INTRODUCTION

The nuances of superconducting states derived from topological insulators have attracted significant attention in the recent past and have provided a fertile testing ground for several emergent phenomena associated with quantum condensed matter [1]. Along with nontrivial bulk wave functions, topological superconductors are associated with a set of symmetry principles and are predicted to host unconventional superconductivity [2]. A topological insulator is characterized by an insulating bulk and gapless conducting surface states. In analogy, a topological superconductor is assigned to be fully gapped in bulk along with gapless surface Andreev bound states [3]. Such exotic field-theoretic ideas have provided the material basis for the realization of Majorana fermions and their projected usage in quantum computers [4]. Experimentally, on the other hand, the onset of superconductivity in the metal intercalated 3D topological insulator Bi_2Se_3 has provided access to decipher pairing and order parameter symmetry in topological superconductors [5–9]. However, the evidence for Andreev surface states in Cu, Sr, and Nb intercalated Bi_2Se_3 superconductors has remained controversial [10]. In particular, in the case of $Sr_{0.1}Bi_2Se_3$, photo-emission measurements have implied an isolated Dirac cone near the Fermi level, without any intervening bulk states [11–13]. The linear dispersion of the surface state near the Dirac cone stems from the spin-momentum locking due to Rashba-type spin-orbit coupling (SOC) [14]. In a typical Rashba-type SOC in other 2D electron gases, the corresponding Fermi surface splits into two counterhelical pockets and mixing of singlet and triplet superconductivity with associated time-reversal symmetry breaking (TRSB) is expected. However, owing to the Z_2 bulk topology, the surface states of $Sr_{0.1}Bi_2Se_3$ host only a single helical Fermi pocket. In such a Fermi surface topology, it is well known that only a singlet pair $(\mathbf{k}\uparrow, -\mathbf{k}\downarrow)$ is allowed ($\mathbf{k}$ is momentum and $\uparrow/\downarrow$ are spins). Moreover, since its spin-flip partner, i.e, $(\mathbf{k}\downarrow, -\mathbf{k}\uparrow)$ is absent in the single helical surface state, the antisymmetric requirement of the pair wave function prescribes that the order parameter must be odd parity. The resulting order parameter, therefore, follows the underlying time-reversal symmetry (TRS) [15].

Theoretically, materials having a trigonal and hexagonal crystal structure with strong SOC are expected to be susceptible toward rotational or spin-rotational symmetry breaking. In particular, rotational symmetry breaking and consequent unconventional superconductivity in $Sr_{0.1}Bi_2Se_3$ and $Nb_{0.25}Bi_2Se_3$ have been reported [5,16]. However, the experimental results on the pairing symmetry remain contradictory as both signatures for conventional and unconventional pairing symmetry are reported with different experiments [10, 17–20]. Besides, a fascinating possibility of unconventional pairing mechanism arises with the development of local moments at Cooper pair sites because of the relative phase difference in a multicomponent order parameter. Such possibilities

*Corresponding authors: pabitra.biswas@stfc.ac.uk; tnmydas@gmail.com; spatnaik@mail.jnu.ac.in

and the existence of associated TRSB been evidenced in Sr_2RuO_4 [21] and several other superconductors (specifically the noncentrosymmetric superconductors) [22–32].

In this paper, we summarize the results of Muon spin rotation and relaxation (μSR) measurements on the single crystals of topological superconductor $Sr_{0.1}Bi_2Se_3$. We provide strong evidence for coexisting TRSB states with triplet pairing along with TRS invariant singlet-pairing states. The possible ground behind the existence of the singlet and triplet mixed state is allowed by the symmetry because of the hexagonal wrapping effect and higher order SOC effect which is specific to $Sr_{0.1}Bi_2Se_3$. Based on Ginzburg-Landau theory, we also develop and specify the criterion for such a mixed pairing state and sketch the phase diagram as a function of chemical potential in doped topological superconductors.

II. EXPERIMENTS

Single crystals of $Sr_{0.1}Bi_2Se_3$ used in this study were grown by a modified Bridgeman technique [6]. High-purity constituent elements Bi, Sr, and Se were taken in stoichiometry ratio in a quartz ampoule which was sealed under vacuum (10^{-4} mbar) and then heated at 850° for eight days followed by slow cooling down to 650° at the rate of 10 °C/h. The ampoule was then quenched in ice-cold water. These single-crystalline materials were extensively characterized by structural and magnetic measurements and a superconducting transition temperature (T_c) of ∼2.5 K was ascertained. For the μSR experiments, about 3g of powdered $Sr_{0.1}Bi_2Se_3$ crystals were mounted on a silver sample holder and placed in a dilution refrigerator operating in the temperature range of 0.05–5 K. Muon spin rotation/relaxation measurements were carried out using the MuSR spectrometer [33] of the ISIS facility at the Rutherford Appleton Laboratory, United Kingdom, and the measurements were performed under zero-field (ZF), longitudinal-field (LF), and transverse-field (TF) protocols. In the ZF-μSR experiments, the sample was cooled down to 0.1 K in true ZF conditions to avoid trapping of any stray field and data were collected up to 3.7 K by warming the sample. In the LF-μSR experiments, the sample was cooled down to 1.4 K under different magnetic fields, applied (above T_c) parallel to the initial muon spin polarization. Similarly, in the TF-μSR experiments, the sample was first field cooled to the base temperature (0.09 K) in a magnetic field of 10 mT applied (above T_c) perpendicular to the initial muon spin polarization and μSR spectra were collected up to 3.6 K upon warming the sample. The ZF- and TF-μSR data were analyzed using the software packages MANTID [34] and MUSRFIT [35].

III. RESULTS AND DISCUSSION

The efficacy of the μSR technique toward unraveling aspects of unconventional superconductivity rests on the fact that the magnetic moment associated with Cooper pairs in such cases is nonzero [21–32]. The μSR technique in ZF mode is exceptionally sensitive to small changes in internal fields. It can measure local magnetic fields of the order of $\approx 10\,\mu$T that corresponds to about 10^{-2} of Bohr magnetron (μ_B). ZF-μSR measurements are therefore very useful to

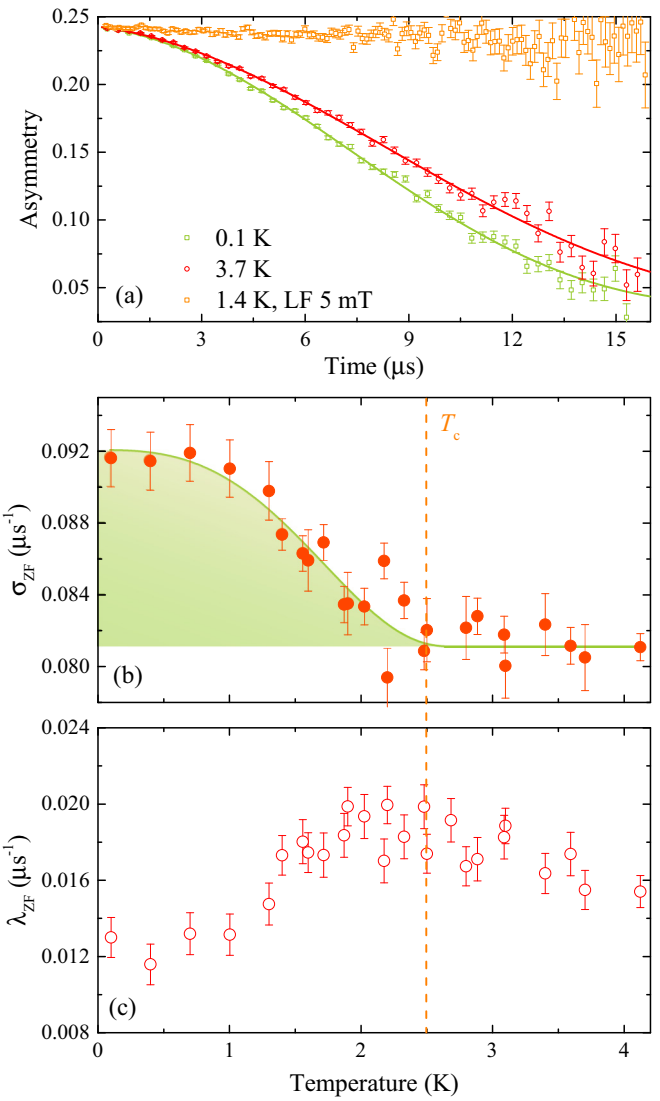

FIG. 1. (a) ZF-μSR spectra collected at 0.1 and 3.7 K and LF-μSR spectra taken at 1.4 K under an LF field of 5 mT. (b), (c) Temperature variation of the relaxation rates σ_{ZF} and λ_{ZF}, indicating spontaneous fields appearing in the superconducting state of $Sr_{0.1}Bi_2Se_3$.

investigate any additional magnetic signal arising spontaneously with the onset of superconductivity. In a typical μSR experiment, 100% spin-polarized muons are embedded onto the sample where they decay within 2.2 μs, giving rise to positrons. The muon spin precesses at the local magnetic environment, and the resultant positrons carry that information into detectors placed in the forward and backward direction of the muon beam. In essence, μSR spectroscopy can reflect signatures of unconventional superconductivity, TRSB, the coexistence of superconductivity and magnetism, along with superconducting pairing symmetry. The asymmetry parameter plotted here is the time-dependent normalized difference function $[A(t) = \frac{N_F(t)-\alpha N_B(t)}{N_F(t)+\alpha N_B(t)}]$ between the number of positrons recorded in the forward detector $N_F(t)$ and backward detector $N_B(t)$. α is the calibration constant which is determined by applying a TF of 20 mT. Figure 1(a) shows the ZF-μSR

spectra for $Sr_{0.1}Bi_2Se_3$ collected at 0.1 and 3.7 K. Also plotted is LF-μSR spectra taken at 1.4 K under a LF of 5 mT. The asymmetry parameter plotted in Fig. 1(a) is the time-dependent normalized difference between the number of positrons recorded in forward and backward detectors. ZF-μSR asymmetry spectra do not show any oscillatory signal which rules out the presence of large internal magnetic fields associated with long-range magnetic order. The ZF-μSR signal collected at 3.7 K (above T_c) shows small relaxation, arising mostly from the nuclear moments of the sample, and also has a temperature-independent background contribution. It is clearly evident that the data collected at 0.1 K (below T_c) shows higher relaxation than that at 3.7 K spectra. The additional relaxation in the asymmetry signal below T_c is due to small spontaneous local fields arising in the superconducting state. Such static magnetic moments are associated with intrinsic Cooper pair magnetization. For a quantitative evaluation of the temperature dependence of the relaxation rate, ZF-μSR data were analyzed using a static Gaussian Kubo-Toyabe relaxation function multiplied by an exponential relaxation function,

$$A(t) = A(0)\left\{\frac{1}{3} + \frac{2}{3}(1-\sigma_{ZF}{}^2t^2)\exp\left(-\frac{\sigma_{ZF}{}^2t^2}{2}\right)\right\} \times \exp(-\lambda_{ZF}) + A_{bg}, \quad (1)$$

where $A(0)$, A_{bg} are the initial and background asymmetries, and σ_{ZF} and λ_{ZF} are muon spin relaxation rates of the randomly orientated nuclear and electronic moments, respectively. The solid lines in Fig. 1(a) are the fits to the data using the above equation.

In the fitting process, both relaxation rates σ_{ZF} and λ_{ZF} were set as free parameters. Figure 1(b) shows the temperature dependence of σ_{ZF} which displays an increase in relaxation rate just below T_c of $\approx$2.5 K. This reconfirms that the spontaneous magnetic fields are emerging in the superconducting state of $Sr_{0.1}Bi_2Se_3$. The appearance of such spontaneous fields just below T_c provides strong evidence for a TRS broken pairing state in $Sr_{0.1}Bi_2Se_3$. In topological insulators, the characteristic topological surface states are protected by TRS, and the TRSB occurs either in a magnetic field or due to the presence of a magnetic entity incorporated with the materials. To rule out the possibility of an impurity-induced relaxation, we have performed additional LF-μSR measurements at 1.4 K. As shown in Fig. 1(a), the application of a small LF field of 5 mT is sufficient to decouple the muon spin from the internal magnetic field. This suggests that the depolarization in the ZF-μSR spectra is caused by weak, static, or quasistatic magnetic fields. Similar TRSB spontaneous magnetic field has also been observed by μSR in Sr_2RuO_4 [21], La_7Rh_3 [22], UPt_3, $(U, Th)Be_{13}$ [24,25], $PrOs_4Sb_{12}$, $Pr(Os_{1-x}Ru_x)_4Sb_{12}$, $PrPt_4Ge_{12}$ [26–28], $LaNiGa_2$ [29], SrPtAs [30], and Re_6Zr [32], etc. Along with an increase in σ_{ZF} below T_c, we also observe a broad hump in the temperature variation of λ_{ZF} at around T_c [see Fig. 1(c)]. A similar humplike feature in $\lambda_{ZF}(T)$ has also been observed in the past in several other TRSB superconductors, such as $Pr_{1-x}Ce_xPt_4Ge_{12}$ [31] and Re_6Zr [32]. While the origin of this additional feature in the $\lambda_{ZF}(T)$ is yet unknown, we speculate that this is happening due to the local inhomogeneity of the spontaneous magnetic moments appearing in the TRSB pairing state.

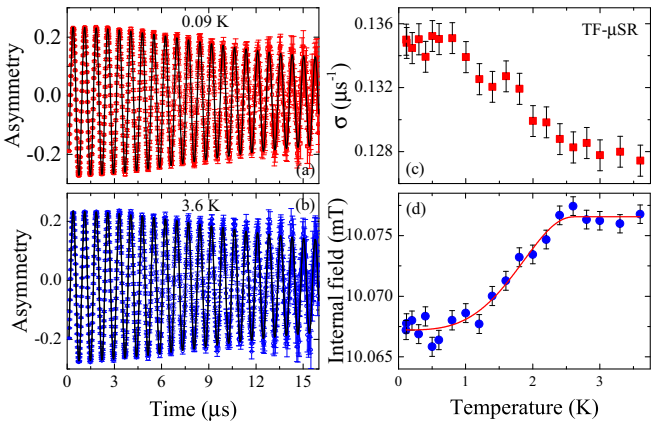

FIG. 2. TF-μSR spectra taken at (a) 0.09 and (b) 3.6 K under 10 mT applied magnetic field. (c) Variation of depolarization rate with temperature. (d) Variation of internal field in the material with temperature.

To understand the pairing symmetry of $Sr_{0.1}Bi_2Se_3$, we have carried out TF-μSR experiments in the superconducting mixed state under an applied magnetic field of 10 mT. Figures 2(a) and 2(b) show the TF-μSR asymmetry spectra for $Sr_{0.1}Bi_2Se_3$ collected at 0.09 K and 3.6 K, respectively. Data collected at 0.09 K shows higher relaxation compared to the normal state at 3.6 K due to inhomogeneous field distribution of flux-line lattice. The solid lines in Figs. 2(a) and 2(b) are the fits to the data using a simple Gaussian-type oscillatory distribution function,

$$A^{TF}(t) = A(0)\exp\left(\frac{-\sigma^2t^2}{2}\right)\cos(\gamma_\mu B_{int}t + \phi) + A_{bg}(0)\cos(\gamma_\mu B_{bg}t + \phi), \quad (2)$$

where $A(0)$ and $A_{bg}(0)$ are the initial asymmetries of the sample and background signals, $\gamma_\mu/2\pi = 135.5$ MHz/T is the muon gyromagnetic ratio [36], B_{int} and B_{bg} are the internal and background magnetic fields, ϕ is the initial phase of the muon precession signal, and σ is the Gaussian muon spin relaxation rate.

The formation of the flux-line lattice is evident from the enhancement of relaxation rate σ observed below transition temperature 2.5 K [Fig. 2(c)]. The temperature dependence of the internal field shown in Fig. 2(d) displays a diamagnetic shift in the field distribution just below T_c, a clear sign of superconductivity in this material. The total sample relaxation rate σ comes from two contributions, the superconducting part σ_{sc} due to the formation of vortex lattice and the nonsuperconducting part σ_{nm} due to the presence of nuclear dipole moments in the material. The latter is expected to be constant over the temperature range of this study. The superconducting component of the relaxation is obtained by quadratically subtracting the background nuclear dipolar relaxation rate obtained from TF-μSR spectra above T_c as $\sigma = \sqrt{\sigma_{sc}^2 + \sigma_{nm}^2}$.

The temperature dependence of the magnetic penetration depth $\lambda(T)$ can be reconstructed from $\sigma_{sc}(T)$ by the simplified

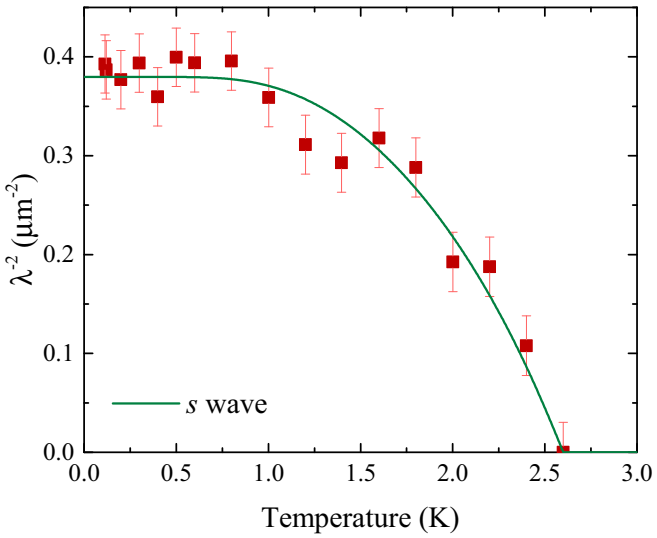

FIG. 3. Variation of λ^{-2} as a function of temperature for $Sr_{0.1}Bi_2Se_3$. Solid lines are the fit to the data using s-wave model.

Brandt equation [37],

$$\frac{\sigma_{sc}(T)}{\gamma_\mu} = 0.06091\frac{\Phi_0}{\lambda^2(T)}, \quad (3)$$

where $\Phi_0 = 2.068 \times 10^{-15}$ Wb is the flux quantum. The above equation is valid when the applied field $H \ll H_{c2}$, where H_{c2} is the upper critical field. $\lambda^{-2}(T)$ is proportional to the effective superfluid density, $\rho_s \propto \lambda^{-2} \propto n_s/m^*$ (n_s is the charge carrier concentration and m^* is the effective mass of the charge carriers), and hence bears the signature of the symmetry of the superconducting gap. Figure 3 shows the temperature dependence of λ^{-2} and hence the superfluid density for $Sr_{0.1}Bi_2Se_3$. The superfluid density shows saturation below $T_c/3$, which in turn suggests the absence of low-lying excitations close to zero temperature that indicates nodeless superconductivity in $Sr_{0.1}Bi_2Se_3$. To get a quantitative estimate, the $\lambda^{-2}(T)$ data were fitted using a single-gap s-, d-, and anisotropic s-wave or two-gap s+s -wave models using the following functional form [38,39]:

$$\frac{\lambda^{-2}(T)}{\lambda^{-2}(0)} = \omega\frac{\lambda^{-2}(T, \Delta_{0,1})}{\lambda^{-2}(0, \Delta_{0,1})} + (1-\omega)\frac{\lambda^{-2}(T, \Delta_{0,2})}{\lambda^{-2}(0, \Delta_{0,2})}, \quad (4)$$

where $\lambda(0)$ is the value of the penetration depth at $T = 0$ K, $\Delta_{0,i}$ is the value of the ith ($i = 1$ or 2) superconducting gap at $T = 0$ K, and ω is the weighting factor of the first gap. Each term in Eq. (4) is evaluated using the standard expression within the local London approximation ($\lambda \gg \xi$) [40,41] as

$$\frac{\lambda^{-2}(T, \Delta_{0,i})}{\lambda^{-2}(0, \Delta_{0,i})} = 1 + \frac{1}{\pi}\int_0^{2\pi}\int_{\Delta_{(T,\varphi)}}^{\infty}\left(\frac{\partial f}{\partial E}\right)\frac{EdEd\varphi}{\sqrt{E^2 - \Delta_i(T,\varphi)^2}}, \quad (5)$$

where $f = [1 + \exp(E/k_BT)]^{-1}$ is the Fermi function, φ is the angle along the Fermi surface, and $\Delta_i(T, \varphi) = \Delta_{0,i}\delta(T/T_c)g(\varphi)$, where $g(\varphi)$ describes the angular dependence of the gap and it is 1 for s- and $s+s$-wave gaps, $|\sin(\varphi/2)|$ for p-wave gap, $|\cos(2\varphi)|$ for d-wave gap, and $(s + \cos 4\varphi)$ for anisotropic s-wave gap.

TABLE I. Fitted parameters to the $\lambda^{-2}(T)$ data of $Sr_{0.1}Bi_2Se_3$ using the different models as described in the text.

Model	Gap value (MeV)	χ^2
s-wave	$\Delta = 0.49(4)$	1.40
$s+s$-wave	$\Delta_1 = 0.7(3)$, $\Delta_2 = 0.3(1)$, and $\omega = 0.58(8)$	1.06
Anisotropic s-wave	$\Delta = 0.54(6)$ with $s = 0.6(2)$	1.02
p-wave	$\Delta = 0.55(3)$	4.27
d-wave	$\Delta = 0.4(1)$	3.53

An approximation to $\Delta(T)$ can be written as $\delta(T/T_c) = \tanh\{1.82[1.018(T_c/T - 1)]^{0.51}\}$ [38].

The solid curve, shown in Fig. 3, is the fit to the $\lambda^{-2}(T)$ data using s-wave model. For simplicity, we do not show the fit curves from the other models in Fig. 3. All the fitted parameters are summarized in Table I and the fitted curves with respect to the different models are shown in the Supplemental Material [42]. Both anisotropic s-wave and two-gap $s+s$-wave-gap models give better $\chi^2_{reduced}$ value and hence give the best fit to the data compared to any other models mentioned above. We emphasize that recent scanning tunneling microscopy measurements show two-gap s+s-wave and anisotropic s-wave pairing symmetry as the prominent pairing mechanism [19]. For single-gap nodeless pairing, we estimate $\Delta = 0.49(4)$ MeV. The value of the gap to T_c ratio Δ/κ_BT_c is 2.18, which is significantly higher than the BCS value of 1.76. The possibility of $p_x + ip_y$ pairing symmetry with two gaps, one corresponding to singlet (real part) and another corresponding to triplet (imaginary part) pairing symmetry can also be considered. The possible existence of even singlet parity, i.e., the real part of $p_x + ip_y$ pairing symmetry, can be accented from the observation of nodeless superconductivity yielded from penetration depth analysis while the existence of the odd parity triplet part, i.e., the imaginary part of $p_x + ip_y$ pairing symmetry, can be concluded from the TRSB observed in ZF muon spectroscopy. Here, the outcomes of ZF and TF muon spectroscopy results provide very strong ground for the possible existence of $p_x + ip_y$ pairing symmetry, which in turn justifies the prediction of odd parity p-wave pairing symmetry in topological superconductors. Within the present statistical accuracy, it is implied that $Sr_{0.1}Bi_2Se_3$ may not have the extended nodes in the gap function. The absolute value of the magnetic penetration depth $\lambda(0)$ is calculated to be 1622(134) nm, which is in close agreement with the previously documented experimental value [6]. The remarkably large value of $\lambda(0)$ indicates the presence of very low superconducting carrier density, a common feature in this class of topological superconductors.

In summary, while our TF-μSR data that probe temperature-dependent penetration depth around vortices reflect nodeless superconductivity, the ZF-μSR results that probe small moments associated with Cooper-pairs indicate odd-parity pairing. Such singlet-triplet mixing is common in a superconductor with additional symmetry breaking such as noncentrosymmetric superconductors [24–26,29,32,35]. In the following, we develop a phenomenological theory for this observation with regard to topological superconductivity.

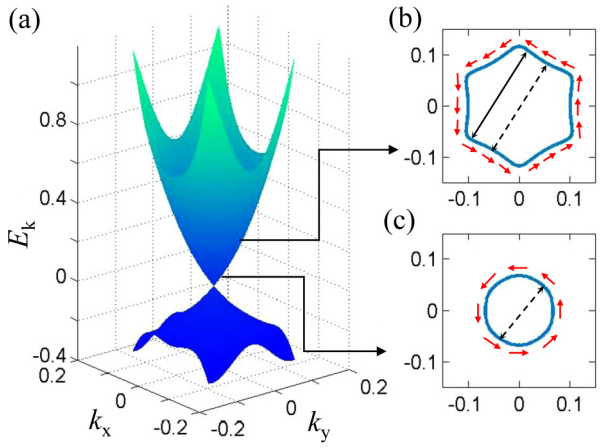

FIG. 4. (a) Single helical surface state of a 3D topological insulator in the $k_x - k_y$-plane. (b), (c) Constant energy cuts (b) far from the Dirac cone and (c) close to the Dirac cone. Red arrows show the corresponding spin alignments across the corresponding constant energy contours. Dashed arrows dictated the k and $-k$ points in which spin is antiparallel, while the solid arrows show similar points where antiparallel alignment of the spin is weakened due to higher order SOC and hexagonal warping effects.

IV. THEORETICAL ANALYSIS

Theory: In several superconductors, especially in noncentrosymmetric materials with Rashba-type SOC, coexistence of singlet- and triplet-pairing symmetries with TRSB has been observed before [24–26,29,32,35]. However, the surface states of $Sr_{0.1}Bi_2Se_3$ can only host a single helical Fermi pocket that would result in odd-parity TR invariant superconductivity. Therefore, the experimental observation of the TRS breaking pairing demands a theoretical explanation which is beyond the existing understanding.

In $Sr_{0.1}Bi_2Se_3$, the chemical potential lies far above the Dirac cone. It is well established that the spin-momentum locking weakens as the chemical potential moves the Dirac point, due to hexagonal warping effects [43] as well as higher order SOC effects [44]. As a combined effect, as one moves away from the Dirac cone, the Fermi surface deviates from circular to snowflake type [see Fig. 4(a)]. The corresponding spin texture becomes more anisotropic, as measured by photoemission spectroscopy [45]. This means the spin of the electrons at a momentum $\pm\mathbf{k}$ away from the diagonal directions [shown by solid arrow in Fig. 4(b)] are no longer antiparallel to each other. In a perfectly helical circular Fermi surface, as in Fig. 4(c), since the spins at $\pm\mathbf{k}$ are antiparallel to each other, only a TR invariant, spin-singlet $(\mathbf{k}\uparrow, -\mathbf{k}\downarrow)$ Cooper pair is allowed here [15]. In the warped Fermi surface in Fig. 4(b), the Cooper pairs across the dashed arrow remain as before. However, the pairs across the tip of the warped Fermi surface, as indicated by the solid arrow, no longer posses antiparallel spin. Therefore, for these electrons, both spin singlet $(\uparrow\downarrow)$ and spin-triplet $(\uparrow\uparrow, \downarrow\downarrow)$ pairings become favorable by symmetry. Hence a triplet pairing with TRSB gains dominance as the chemical potential is moved above the Dirac point, which is the case in the present system.

The warped surface state and its unconventional spin texture can be realistically modeled by a low-energy Hamiltonian [44] $H(\mathbf{k}) = \xi_{\mathbf{k}}\mathbf{I}_{2\times2} + \mathbf{d}_{\mathbf{k}}\cdot\sigma$, with σ being the 2×2 Pauli matrices. The on-site dispersion $\xi_{\mathbf{k}} = k^2/m_1 + k^4/m_2$, with $k = |\mathbf{k}|$. The off-diagonal gap terms are $d_x = -\alpha_{\mathbf{k}}k_y - \mathrm{Im}[\beta_{\mathbf{k}}]$ and $d_y = \alpha_{\mathbf{k}}k_x - \mathrm{Re}[\beta_{\mathbf{k}}]$, where $\alpha_{\mathbf{k}} = \alpha_0 + \alpha_1k^2 + \alpha_2k^4$ and $\beta_{\mathbf{k}} = \beta_0[(k_+^5 + k_-^5) + i(k_+^5 - k_-^5)]$ are the first- and fifth-order Dresselhaus SOC coefficients, where $k_\pm = k_x \pm ik_y$. The structural warping term gives an Ising-like, anisotropic spin-splitting as $d_z(\mathbf{k}) = \lambda_{\mathbf{k}}(k_+^3 + k_-^3)$, with $\lambda_{\mathbf{k}} = \lambda_0 + \lambda_1k^2$. All parameters are obtained by fitting to the experimental Fermi surface warping and the anomalous spin-texture as given in Refs. [43,44,46]. Clearly, the SOC term $d_{||} = \sqrt{d_x^2 + d_y^2}$ provides the helicity to the electron's spin-momentum relationship, while the warping term d_z opposes it. Clearly, $d_{||}$ promotes the spin-singlet pairing, while d_z helps to stablize the spin-triplet pairing.

The superconductivity is expected to have odd-parity symmetry, so it makes sense to study its unconventional pairing mechanism. Since the spins are locked to the in-plane momentum, the relevant interaction term consists of Hubbard interaction and/or an XY-type Heisenberg term for the spin-singlet pairing, and a Dyzoloshinskii-Moriya (DM) term for the spin-triplet pairing. The net interaction term is

$$H_{\mathrm{int}} = \sum_{i\neq j}[Un_{i\uparrow}n_{i,\downarrow} + J\mathbf{S}_i\cdot\mathbf{S}_j + i\mathbf{D}\cdot(\mathbf{S}_i\times\mathbf{S}_j)], \quad (6)$$

where U is the Hubbard interaction, J and $\mathbf{D}$ are the nearest-neighbor symmetric and antisymmetric (DM) spin-exchange terms, respectively. $n_{i,\sigma}$, and $\mathbf{S}_i$ are the number and spin-density operators, respectively, at a given site i, with spin $\sigma = \uparrow, \downarrow$. Given that spin is confined only in the x, y plane, we set $\mathbf{D} = D_z\hat{z}$. Expanding the density and spin operators in terms of fermionic creation and annihilation operators $c^\dagger_{\mathbf{k},\sigma}$, $c_{\mathbf{k},\sigma}$, and using Hubbard-Stratonovic transformation, we obtain the singlet and triplet superconducting (SC) order parameters [42], defined as

$$\Delta_s(\mathbf{k}) = \sum_{\mathbf{k}'} u_s(\mathbf{k},\mathbf{k}')\langle c_{-\mathbf{k}',\downarrow}c_{\mathbf{k}',\uparrow}\rangle, \quad (7)$$

$$\Delta_t(\mathbf{k}) = \sum_{\mathbf{k}'} u_t(\mathbf{k},\mathbf{k}')\langle c_{-\mathbf{k}',\uparrow}c_{\mathbf{k}',\uparrow}\rangle. \quad (8)$$

$c_{\mathbf{k},\sigma}$ is the annihilation operator of electron at momentum $\mathbf{k}$, with spin σ. The singlet- and triplet-pairing potential can be easily read as $u_s(\mathbf{k},\mathbf{k}') = (Us_{\mathbf{k}} - Js_{-\mathbf{k}})s_{\mathbf{k}'}$ and $u_t(\mathbf{k},\mathbf{k}') = D_zt_{\mathbf{k}}t_{\mathbf{k}'}$, where $s_{\mathbf{k}}$ and $t_{\mathbf{k}}$ are the structure factors for the singlet and triplet pairings. As discussed before, both $s_{\mathbf{k}}$ and $t_{\mathbf{k}}$ must be odd under parity. It is easy to verify that due to the odd-parity nature of the pairing symmetry, Δ_s is TR invariant, while Δ_t breaks this symmetry. We note that, owing to rhombohedral structure of this compound, the irreducible representation is reduced from sixfold symmetry to the threefold C_{3v} class. This also reflects in the SC order parameter, and can be a candidate explanation to the in-plane rotational symmetry breaking as observed before [16].

With an eye on the experimental observation, we are here mainly interested in unravelling the phase diagram between the Δ_s, and Δ_t order parameters as a function of chemical potential tuning. The phase competition between the two order parameters can be understood within the Ginzburg-Landau

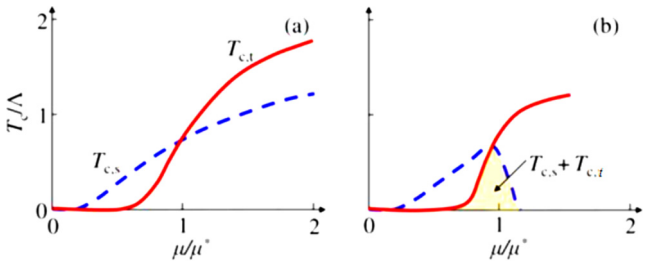

FIG. 5. (a) Two superconducting transition temperatures for the singlet ($T_{c,s}$) and triplet ($T_{c,t}$) pairings, assuming same coupling constant $u_s = u_t$ but different density of states. The cross terms in the free energy (γ, δ) are neglected. (b) As the cross terms are introduced, both phases become complementary, with a small region of their coexistence near the tricritical point μ^*.

framework, in which the free energy can be expanded in terms of the order parameters as [42]

$$F = \alpha_s|\Delta_s|^2 + \alpha_t|\Delta_t|^2 + \frac{\beta_s}{2}|\Delta_t|^4 + \frac{\beta_t}{2}|\Delta_t|^4 + \frac{\gamma_s}{2}(\Delta_s\Delta_t^*)^2 + \frac{\gamma_t}{2}(\Delta_s^*\Delta_t)^2 + \delta|\Delta_s|^2|\Delta_t|^2. \quad (9)$$

$i = s, t$ are for singlet and triplet terms, respectively. The full expressions for the expansion parameters α_i, β_i, γ, and δ are given in the Supplemental Material [42]. In the absence of phase competition terms, i.e., when $\gamma = \delta = 0$, the individual phase transition of Δ_i occurs at $\alpha_i = 0$. Near the phase transition, α_i can be evaluated analytically, as $\alpha_i = \frac{1}{u_i} - N_i \log \frac{\Lambda}{T}$ (i = s,t), where Λ is the momentum cutoff. In the leading order terms, we have $N_s \sim \langle d_{||}(\mathbf{k})\rangle_{\mathrm{FS}}$, and $N_t \sim \langle d_z(\mathbf{k})\rangle_{\mathrm{FS}}$. In what follows, N_s is determined by the SOC term $d_{||}$, while N_t depends on the hexagonal warping term d_z. So, N_s dominates near the Dirac cone, while N_t takes over at higher energy. The individual SC transition temperature is $T_{c,i} = \Lambda e^{-1/u_i N_i}$, and its variation with the chemical potential is plotted in Fig. 5(a). From scaling analysis, we can estimate that such transition occurs when the chemical potential becomes $\mu^* \sim \alpha_0 k_F$.

As the phase competition terms $\gamma > 0$ and $\delta > 0$ are turned on, the phase diagram changes as follows. Once again the calculation simplifies at the critical point where $T_c^* = T_{c,s} = T_{c,t}$. At this point, $u_s N_s \approx u_t N_t$, which leads to $N_s/N_t \sim D_z/(U - J)$ at μ^*. In this limit, we also find that $\beta_s = \beta_t = 5\beta$ and $\gamma_s = \gamma_t = \delta = 3\beta$, with $\beta = 7\zeta(3)/64\pi^2(T_c^*)^2$. The free energy is minimum when the $(\Delta_s\Delta_t^*)^2 = -|\Delta_s|^2|\Delta_t|^2$, implying that the phase difference between the two order parameters is $\pi/2$. The free-energy minimization leads to the condition that both phases coexist when $\gamma\delta < \beta_s\beta_t$ [47]. Since this condition is satisfied near T_c^*, we conclude that the singlet to triplet phase transition is intervened by a region of their uniform coexistence. Based on these results, we draw the over phase diagram as shown in Fig. 5(b).

V. CONCLUSION

In summary, we have performed the ZF and TF μSR measurements on topological superconductor $Sr_{0.1}Bi_2Se_3$. The μSR measurements in ZF mode unveil the presence of triplet pairing with unambiguous evidence for TRSB. The TF μSR measurement, on the other hand, yields the presence of low carrier density, nodeless superconductivity, and the zero-temperature penetration depth is estimated to be $\lambda(0) = 1622(134)$ nm. Theoretically, the existence of triplet pairing is defined in terms of hexagonal wrapping effect with higher order Dresselhaus SOC terms. Under the framework of Ginzburg-Landau theory, the coexistence of singlet and triplet pairing is indicated in terms of chemical potential tuning. Our observation of TRSB states in a class of topological superconductors is a surprising development that promises insight into superconducting states derived from topological insulators.

ACKNOWLEDGMENTS

P.N. thanks University Grant Commission (UGC) for providing a Basic Science Research (BSR) fellowship. S.P. acknowledges DST FIST and DST PURSE programs for supporting the low-temperature high magnetic field facility at Jawaharlal Nehru University and also financial support received from SERB extra mural grant (EMR/2016/003998/PHY) and DST (INT/RUS/RFBR/P-316), Government of India. P.N. and S.P. thank Rutherford Appleton Laboratory for providing Newton Bhabha funding for the Muon spectroscopy measurements. T.D. acknowledges financial support from the DST, India under the Start Up Research Grant (Young Scientist) [SERB No. YSS/2015/001286], and from the Infosys Young Investigator award. We thank Shiv Kumar (Hiroshima Syncrotron Center, Hiroshima University, Japan) and K. Ashokan (Inter University Accelerator Center, New Delhi, India) for ARPES measurements.

[1] M. Z. Hasan and C. L. Kane, Rev. Mod. Phys. **82**, 3045 (2010).
[2] L. Chirolli, F. de Juan, and F. Guinea, Phys. Rev. B **95**, 201110(R) (2017).
[3] X.-L. Qi and S.-C. Zhang, Rev. Mod. Phys. **83**, 1057 (2011).
[4] S. Das Sarma, M. Freedman, and C. Nayak, Quantum Inf. **1**, 15001 (2015).
[5] Y. Pan, A. M. Nikitin, G. K. Araizi, Y. K. Huang, Y. Matsushita, T. Naka, and A. de Visser, Sci. Rep. **6**, 28632 (2016).
[6] Z. T. Tang, J. K. Bao, Y. Liu, Y. L. Sun, A. Ablimit, H. F. Zhai, H. Jiang, C. M. Feng, Z. A. Xu, and G. H. Cao, Phys. Rev. B **91**, 020506(R) (2015).
[7] Z. Liu, H. Yao, J. Shao, M. Zuo, L. Pi, S. Tan, C. Zhang, and Y. Zhang, J. Am. Chem. Soc. **137**, 10512 (2015).
[8] Y. Qiu, K. N. Sanders, J. Dai, J. E. Medvedeva, W. Wu, P. Ghaemi, T. Vojta, and Y. S. Hor, arXiv:1512.03519.
[9] Y. S. Hor, A. J. Williams, J. G. Checkelsky, P. Roushan, J. Seo, Q. Xu, H. W. Zandbergen, A. Yazdani, N. P. Ong, and R. J. Cava, Phys. Rev. Lett. **104**, 057001 (2010).

[10] S. Sasaki, M. Kriener, K. Segawa, K. Yada, Y. Tanaka, M. Sato, and Y. Ando, Phys. Rev. Lett. **107**, 217001 (2011).

[11] L. A. Wray, S.-Y. Xu, Y. Xia, Y. S. Hor, D. Qian, A. V. Fedorov, H. Lin, A. Bansil, R. J. Cava, and M. Z. Hasan, Nat. Phys. **6**, 855 (2010).

[12] Y. Tanaka, K. Nakayama, S. Souma, T. Sato, N. Xu, P. Zhang, P. Richard, H. Ding, Y. Suzuki, P. Das, K. Kadowaki, and T. Takahashi, Phys. Rev. B **85**, 125111 (2012).

[13] C. Q. Han, H. Li W. J. Chen, F. Zhu, Meng-Yu Yao, Z. J. Li, M. Wang, Bo F. Gao, D. D. Guan, C. Liu, C. L. Gao, D. Qian, and Jin-Feng Jia, Appl. Phys. Lett. **107**, 171602 (2015).

[14] B. Andrei Bernevig, *Topological Insulators and Topological Superconductors* (Princeton University Press, Princeton, New Jersey, 2013).

[15] L. Fu and E. Berg, Phys. Rev. Lett. **105**, 097001 (2010); M. Sato, Phys. Rev. B **81**, 220504(R) (2010).

[16] T. Asaba, B. J. Lawson, C. Tinsman, L. Chen, P. Corbae, G. Li, Y. Qiu, Y. S. Hor, Liang Fu, and Lu Li, Phys. Rev. X **7**, 011009 (2017).

[17] N. Levy, T. Zhang, J. Ha, F. Sharifi, A. A. Talin, Y. Kuk, and J. A. Stroscio, Phys. Rev. Lett. **110**, 117001 (2013).

[18] K. Kirshenbaum, P. S. Syers, A. P. Hope, N. P. Butch, J. R. Jeffries, S. T. Weir, J. J. Hamlin, M. B. Maple, Y. K. Vohra, and J. Paglione, Phys. Rev. Lett. **111**, 087001 (2013).

[19] G. Du, J. Shao, X. Yang, Z. Du, D. Fang, J. Wang, K. Ran, J. Wen, C. Zhang, H. Yang, Y. Zhang, and H. H. Wen, Nat. Commun. **8**, 14466 (2015).

[20] T. V. Bay, T. Naka, Y. K. Huang, H. Luigjes, M. S. Golden, and A. de Visser, Phys. Rev. Lett. **108**, 057001 (2012).

[21] G. M. Luke, Y. Fudamoto, K. M. Kojima, M. I. Larkin, J. Merrin, B. Nachumi, Y. J. Uemura, Y. Maeno, Z. Q. Mao, Y. Mori, H. Nakamura, and M. Sigrist, Nature (London) **394**, 558 (1998).

[22] D. Singh, M. S. Scheurer, A. D. Hillier, and R. P. Singh, arXiv:1802.01533.

[23] J. A. T. Barker, D. Singh, A. Thamizhavel, A. D. Hillier, M. R. Lees, G. Balakrishnan, D. McK. Paul, and R. P. Singh, Phys. Rev. Lett. **115**, 267001 (2015).

[24] G. M. Luke, A. Keren, L. P. Le, W. D. Wu, Y. J. Uemura, D. A. Bonn, L. Taillefer, and J. D. Garrett, Phys. Rev. Lett. **71**, 1466 (1993).

[25] R. H. Heffner, J. L. Smith, J. O. Willis, P. Birrer, C. Baines, F. N. Gygax, B. Hitti, E. Lippelt, H. R. Ott, A. Schenck, E. A. Knetsch, J. A. Mydosh, and D. E. MacLaughlin, Phys. Rev. Lett. **65**, 2816 (1990).

[26] Y. Aoki, A. Tsuchiya, T. Kanayama, S. R. Saha, H. Sugawara, H. Sato, W. Higemoto, A. Koda, K. Ohishi, K. Nishiyama, and R. Kadono, Phys. Rev. Lett. **91**, 067003 (2003).

[27] L. Shu, W. Higemoto, Y. Aoki, A. D. Hillier, K. Ohishi, K. Ishida, R. Kadono, A. Koda, O. O. Bernal, D. E. MacLaughlin, Y. Tunashima, Y. Yonezawa, S. Sanada, D. Kikuchi, H. Sato, H. Sugawara, T. U. Ito, and M. B. Maple, Phys. Rev. B **83**, 100504(R) (2011).

[28] A. Maisuradze, W. Schnelle, R. Khasanov, R. Gumeniuk, M. Nicklas, H. Rosner, A. Leithe-Jasper, Yu. Grin, A. Amato, and P. Thalmeier, Phys. Rev. B **82**, 024524 (2010).

[29] A. D. Hillier, J. Quintanilla, B. Mazidian, J. F. Annett, and R. Cywinski, Phys. Rev. Lett. **109**, 097001 (2012).

[30] P. K. Biswas, H. Luetkens, T. Neupert, T. Stürzer, C. Baines, G. Pascua, A. P. Schnyder, M. H. Fischer, J. Goryo, M. R. Lees, H. Maeter, F. Brückner, H.-H. Klauss, M. Nicklas, P. J. Baker, A. D. Hillier, M. Sigrist, A. Amato, and D. Johrendt, Phys. Rev. B **87**, 180503(R) (2013).

[31] J. Zhang, D. E. MacLaughlin, A. D. Hillier, Z. F. Ding, K. Huang, M. B. Maple, and Lei Shu, Phys. Rev. B **91**, 104523 (2015).

[32] R. P. Singh, A. D. Hillier, B. Mazidian, J. Quintanilla, J. F. Annett, D. McK. Paul, G. Balakrishnan, and M. R. Lees, Phys. Rev. Lett. **112**, 107002 (2014).

[33] http://www.isis.stfc.ac.uk/instruments/musr

[34] http://www.mantidproject.org

[35] A. Suter and B. M. Wojek, Physics Procedia **30**, 69 (2012).

[36] J. E. Sonier, J. H. Brewer, and R. F. Kiefl, Rev. Mod. Phys. **72**, 769 (2000).

[37] E. H. Brandt, Phys. Rev. B **37**, 2349(R) (1988).

[38] A. Carrington, and F. Manzano, Physica C **385**, 205 (2003).

[39] H. Padamsee, J. E. Neighbor, and C. A. Shiffman, J. Low. Temp. Phys. **12**, 387 (1973).

[40] M. Tinkham, *Introduction to Superconductivity* (McGraw-Hill, New York, 1975).

[41] R. Prozorov and R. W. Giannetta, Supercond. Sci. Technol. **19**, R41 (2006).

[42] See Supplemental Material at http://link.aps.org/supplemental/10.1103/PhysRevMaterials.3.074201 for a brief background to theoretical analysis on the superconducting state derived from topological insulators and also additional experimental data on basic characterization of the sample including ARPES and magnetic susceptibility. The fully gapped spin-triplet pairing channel is developed from microscopic theory.

[43] L. Fu, Phys. Rev. Lett. **103**, 266801 (2009).

[44] S. Basak, H. Lin, L. A. Wray, S.-Y. Xu, L. Fu, M. Z. Hasan, and A. Bansil, Phys. Rev. B **84**, 121401(R) (2011).

[45] Y. H. Wang, D. Hsieh, D. Pilon, L. Fu, D. R. Gardner, Y. S. Lee, and N. Gedik, Phys. Rev. Lett. **107**, 207602 (2011).

[46] The values of the parameters are obtained by fitting the Fermi surface as well as the spin texture of Bi_2Te_3 as obtained by ARPES measurements [44]. The parameters are $m_1 = 70.42\,\mathrm{eV}^{-1}\,\mathrm{Å}^{-2}$, $m_2 = 76.92\,\mathrm{eV}^{-1}\,\mathrm{Å}^{-4}$, $\alpha_0 = -5\times10^{-4}\,\mathrm{eV\,Å}$, $\alpha_1 = -74\times10^{-4}\,\mathrm{eV\,Å}^3$, $\alpha_2 = 6.3\times10^{-4}\,\mathrm{eV\,Å}^5$, $\lambda_0 = -0.04\,\mathrm{eV\,Å}^3$, $\lambda_1 = 4\times10^{-5}\,\mathrm{eV\,Å}^5$, and $\zeta = 0.35\,\mathrm{eV\,Å}^5$.

[47] R. M. Fernandes, and Jörg Schmalian, Phys. Rev. B **82**, 014521 (2010); T. Das, *ibid.* **87**, 144505 (2013); M. Khodas and A. V. Chubukov, Phys. Rev. Lett. **108**, 247003 (2012); Y. Wang and L. Fu, *ibid.* **119**, 187003 (2017).